



RESEARCH ARTICLE

10.1029/2023JD038481

Key Points:

- The effective radiative forcing (ERF) of sulfate-black carbon (SBC) composite species in GFDL AM4 model ranges from -0.51 ± 0.1 to $-1.06 \pm 0.1 \text{ W m}^{-2}$
- The broad range is attributed to the choice of emissions and the permitted influence of the other aerosol species
- Over East China, the choice of the emission condition for organic carbon (present-day or preindustrial) modulates the ERF of SBC by 37%

Supporting Information:

Supporting Information may be found in the online version of this article.

Correspondence to:

G. Govardhan,
gaurav.govardhan@tropmet.res.in

Citation:

Govardhan, G., Paynter, D., & Ramaswamy, V. (2023). Effective radiative forcing of the internally mixed sulfate and black carbon aerosol in the GFDL AM4 model: The role played by other aerosol species. *Journal of Geophysical Research: Atmospheres*, 128, e2023JD038481. <https://doi.org/10.1029/2023JD038481>

Received 3 JAN 2023

Accepted 17 OCT 2023

Author Contributions:

Conceptualization: Gaurav Govardhan, David Paynter, Venkatachalam Ramaswamy

Data curation: Gaurav Govardhan

Formal analysis: Gaurav Govardhan

Investigation: Gaurav Govardhan, David Paynter, Venkatachalam Ramaswamy

Methodology: Gaurav Govardhan, David Paynter, Venkatachalam Ramaswamy

Project Administration: Venkatachalam Ramaswamy

© 2023 The Authors.

This is an open access article under the terms of the [Creative Commons Attribution-NonCommercial License](https://creativecommons.org/licenses/by-nc/4.0/), which permits use, distribution and reproduction in any medium, provided the original work is properly cited and is not used for commercial purposes.

Effective Radiative Forcing of the Internally Mixed Sulfate and Black Carbon Aerosol in the GFDL AM4 Model: The Role Played by Other Aerosol Species

Gaurav Govardhan^{1,2} , David Paynter¹ , and Venkatachalam Ramaswamy^{1,2}

¹NOAA Geophysical Fluid Dynamics Laboratory, Princeton, NJ, USA, ²Atmospheric and Oceanic Sciences Program, Princeton University, Princeton, NJ, USA

Abstract We compute the effective radiative forcing (ERF) of the internally mixed sulfate-black carbon (SBC) aerosol species in the Geophysical Fluid Dynamics Laboratory's (GFDL) Atmospheric Model version 4 (AM4) model using five different formulations. The formulations differ in how they account for the presence of other aerosol species. The global mean ERF of SBC in the GFDL AM4 model ranges from -0.51 ± 0.1 to $-1.06 \pm 0.1 \text{ W m}^{-2}$. The three most realistic configurations of the five, in which the emissions of other aerosol species vary between 1850 and 2010 states, depict a tighter distribution of ERF (-0.51 , -0.55 , and -0.57 ± 0.1). The two outlier configurations completely exclude one or more other aerosol species, which is slightly unrealistic but included for completeness. The former three configurations, however, result in substantially different ERFs over the regional hot spots of aerosols, e.g., over the land-mass of East China; the choice of the emission conditions for organic carbon (i.e., present-day or preindustrial) affects the ERF of SBC by $\sim 37\%$. The component of ERF related to aerosol-cloud interactions (ACI) gets principally affected by the presence of other aerosol species. The higher the emissions of other aerosol species, the lesser is the ERF of SBC associated with ACI. This finding suggests that for ERF estimates, the choice of the emission level/concentrations of the other aerosol species significantly affects the estimates of SBC, especially over the aerosol hot spots.

Plain Language Summary The radiative imbalance at the top-of-the-atmosphere caused by the changes in the anthropogenic emissions of aerosols from preindustrial (PI) times to the present-day (PD), with the oceanic conditions held constant, is termed as the effective radiative forcing (ERF) of anthropogenic aerosols on the earth system. In this study, using the Geophysical Fluid Dynamics Laboratory's (GFDL) Atmospheric Model version 4 (AM4) model, we show that the ERF of the individual aerosol species depends upon the prescription of the emission levels of the other aerosol species. For instance, the prescription of emissions or organic carbon aerosol to PI and PD values changes the ERF of sulfate-black carbon (SBC) composite species by 37% over eastern China. This dependence principally arises from the aerosol-cloud interaction, while aerosol-radiation interactions are relatively independent of the emission levels of the other aerosol species. Nevertheless, on a global mean basis, this dependence of ERF of SBC on the emissions of other anthropogenic aerosols is much weak.

1. Introduction

The response of the climate system to the increasing greenhouse gas emissions has a broad range, as established by many previous studies (Knutti et al., 2017; Zelinka et al., 2014, 2020). Apart from many other factors, it also depends upon the forcing strength of and the system's response to the other anthropogenic agents (Stevens, 2015). The uncertainty in the response of the climate system to the anthropogenic forcing, though arising partly due to the varying climate feedback across the different models, also stems from the uncertainty in the magnitudes of the forcing applied across these models (Andrews, 2014; Chung & Soden, 2015; P. M. Forster et al., 2016; Pincus et al., 2016; Ramaswamy et al., 2019). Of all the anthropogenic agents (well-mixed greenhouse gases, ozone, land use, aerosols, etc.) causing an imbalance in the radiation budget of the earth system (broadly termed as radiative forcing (RF)), aerosols pose the most uncertain forcing (Myhre et al., 2013; Smith et al., 2020; Szopa et al., 2021). However, the importance of aerosol forcing is specifically underscored as it negates a substantial portion of the positive forcing associated with CO₂ and other well-mixed greenhouse gases (Myhre et al., 2013; Smith et al., 2020; Szopa et al., 2021). Of the various definitions of RF (Myhre et al., 2013; Sherwood et al., 2015),

Resources: David Paynter, Venkatachalam Ramaswamy
Software: David Paynter, Venkatachalam Ramaswamy
Supervision: David Paynter, Venkatachalam Ramaswamy
Validation: Gaurav Govardhan
Visualization: Gaurav Govardhan
Writing – original draft: Gaurav Govardhan
Writing – review & editing: David Paynter, Venkatachalam Ramaswamy

effective radiative forcing (ERF) is the most relevant for the estimation of the climate response to the implied forcing (Pincus et al., 2016; Ramaswamy et al., 2019; Sherwood et al., 2015). The present-day (PD) ERF attributed to a particular forcing agent (such as aerosols, land use, greenhouse gases, etc.) is the change in the net radiative flux at the top-of-the-atmosphere (TOA) owing to the change of the forcing agent from a preindustrial (PI) state when sea-surface temperatures (SSTs) are held fixed (Hansen et al., 2005). Unlike the traditional RF definitions, e.g., the instantaneous radiative forcing (IRF) and the stratospherically adjusted RF (Hansen et al., 1997; Myhre et al., 2013; Ramaswamy et al., 2019, and the references therein), the ERF allows for both fast stratospheric and tropospheric adjustments that get triggered as a response to the applied forcing. The Intergovernmental Panel on Climate Change (IPCC), in its 6th Assessment Report (AR6, P. Forster et al., 2021), assessed PI to PD ERF for aerosols as $-1.11 \pm 0.38 \text{ W m}^{-2}$, with $-0.25 \pm 0.40 \text{ W m}^{-2}$ contribution coming from aerosol-radiation interactions (ARI) and the remaining $-0.86 \pm 0.57 \text{ W m}^{-2}$ from aerosol-cloud interactions (ACI). Several studies have focused on understanding the causes behind such a large range in the aerosol ERF (Carslaw et al., 2013; Fiedler et al., 2017; Kretzschmar et al., 2017; Regayre et al., 2014, 2018; Stevens, 2015). One of the main causes behind the uncertainty associated with aerosol ERF is ACI which are heavily dependent on the background aerosols (Carslaw et al., 2013, 2017; Hamilton et al., 2018; Liu et al., 2021; Malavelle et al., 2017; Mülmenstädt & Feingold, 2018; Regayre et al., 2014; Szopa et al., 2021; Wilcox et al., 2015). Other significant sources of uncertainty in aerosol ERF are anthropogenic emissions and aerosol processes (Regayre et al., 2014).

The ERF of aerosols can be further broken down into that of the individual species (e.g., sulfate, black carbon, organic carbon, nitrate, etc.). Such individual ERF values can be analogously computed by using model simulations that employ PD and PI emissions/concentrations of the aerosol species of interest. However, in such simulations, depending upon the choice, the remaining aerosol species could either be set to their PD or their PI state. In this study, we seek to understand the difference between such ERF calculations of the internally mixed sulfate-black carbon (SBC) species, which differ from each other in terms of their prescription of the conditions of the other aerosol species. For that, we use the Geophysical Fluid Dynamics Laboratory's (GFDL) Atmospheric Model version 4 (AM4). It simulates the distribution of five aerosol species, including sulfate (S), black carbon (BC), organic carbon (OC), sea-salt, and mineral dust. However, the optical properties of sulfate and black carbon are internally mixed, making it in essence a single species, that we refer to as SBC. While individually sulfate and black carbon have different sources and formation mechanisms, once in the atmosphere, they are observationally known to have similar residence times (Bondietti & Papastefanou, 1993; Cape et al., 2012; Rasch et al., 2001; Rodhe et al., 1972), and hence they are assumed to be coexistent. Moreover, the assumption about their internal mixture in the GFDL AM4 model is based on the findings of several field studies (e.g., Abel et al., 2003; Martins et al., 1998; Naoe & Okada, 2001; Okada et al., 2005; Pósfai et al., 2003; Russell & Heintzenberg, 2000) conducted to examine the state of mixing of aerosol in the ambient conditions. In this study, we focus on estimating the ERF of SBC, as both sulfate and black carbon individually dominate the anthropogenic aerosol forcing budget, albeit with contrasting behavior. Moreover, the changes in anthropogenic emissions over the 1850 to 2014 period are estimated to most impact SBC (Szopa et al., 2021). We then explore how the changes in the three other species (OC, sea-salt and mineral dust) impact the SBC 2014 ERF. Specifically, we carry out several model experiments by (a) specifying the anthropogenic emissions for OC either to PD (2014) or PI (1850), and (b) excluding combinations of mineral dust, and sea-salt aerosol species (in their 1850 state) from aerosol-radiation and ACI in the model. These latter exclusion experiments aim to understand how the background state of nonanthropogenic aerosol influence SBC ERF. Hence, we further decompose the computed ERFs into their characteristic components, as specified by Ghan (2013), to understand the physical processes responsible for the control of other aerosol species on the ERF of SBC. Lastly, we carry out additional model experiments that hold the direct and indirect effects of aerosols one by one to explicitly see their role in the computed ERF of SBC. We note that the ERF of aerosols could also depend upon the choice of the background climate conditions of SST and sea-ice. However, here, in all cases we focus on the impact of changing other aerosol and keeping the SST and sea-ice in a prescribed 1850 state. In AM4, the natural aerosols (sea-salt and dust) emissions are not prescribed, but are computed based on near-surface wind fields, which are governed by the SST and sea-ice conditions. Hence, changing the SSTs and sea-ice would lead to changes in the background state that would make interpretation of our results less clear. Thus, in this study, we limit our focus to background aerosols. The details about the GFDL AM4 model are described in Section 2. The methodology employed to compute ERFs of SBC with varying conditions of the other aerosol species can also be found in Section 2. The results are discussed in Section 3, while the conclusions are outlined in Section 4.

2. Methodology

2.1. Model Details

The GFDL AM4 model has been utilized for this study. The details about the dynamical core, spatial resolution, physical and chemical parameterization techniques, etc., employed in this newer version of GFDL's family of models have been documented in Zhao et al. (2018a, 2018b) and Held et al. (2019). The model has a horizontal resolution of roughly 100 km and has 33 vertical levels. It simulates the distribution of five aerosol species, including sulfate (S), black carbon (BC), organic carbon (OC), sea-salt, and mineral dust. The details regarding process-level modeling of these species in AM4 appear in Donner et al. (2011), Naik et al. (2013), and Zhao et al. (2018b). The emissions of anthropogenic aerosol species are consistent with that suggested by Hoesly et al. (2018). The aerosol module simulates the aerosol lifecycle in the atmosphere, including emissions, transport, transformation, and deposition.

The shortwave and longwave radiative parameterization schemes in the GFDL AM4.0 model are mainly based on Freidenreich and Ramaswamy (1999) and Schwarzkopf and Ramaswamy (1999), respectively. However, there are a few updates in the physics (Zhao et al., 2018a, 2018b). In the shortwave scheme, these include (a) added parameterizations to account for shortwave absorption due to the CH₄ and N₂O, (b) incorporation of the effects of the shortwave water self-continuum (BPS 2.0), updated foreign continuum from CKD 2.1 to BPS 1.1 (Paynter & Ramaswamy, 2012; Paynter et al., 2014) and added effects of the O₂ and N₂ continua. The major modification in the longwave radiative parameterization is the inclusion of the CO₂ bands in the 990–1,200 cm⁻¹ range (commonly called the 10-μm band).

For the ARI, the aerosol optical properties including extinction efficiency, single-scattering albedo, and asymmetry parameter are calculated on the basis of Mie theory, with the assumptions that all the particles are spherical. Sulfate and carbonaceous aerosols are assumed to be lognormally distributed. The geometric mean radius and standard deviation of the lognormal distribution for sulfate and black carbon are taken from Haywood and Ramaswamy (1998), while that for organics are taken from Hess et al. (1998). The mass size distribution of dust and sea-salt is assumed constant within five bins from 0.1 to 10 μm. Sulfate and black carbon are assumed to be internally mixed for the purpose of ARI. The BC fraction of the total volume of sulfate and hydrophilic BC is computed. The relative humidity level in the model grid and the BC fraction is utilized to pick the optical properties for sulfate and BC species from a “look-up” table. The look-up is a set of precalculated extinction efficiency, single-scattering albedo, and asymmetry parameter as a function of wavelength and relative humidity using Mie theory. The selected values of optical properties are assigned to sulfate and BC. More details about the calculation of the optical properties of aerosols in GFDL models can be found in Ginoux et al. (2006). Finally, all the aerosol species, including SBC, are assumed to be externally mixed with each other.

AM4 employs a prognostic scheme for cloud liquid droplet number concentration (Ming et al., 2007) in which the activation of the droplets depends upon the updraft velocity and aerosol properties (Ming et al., 2006). The aerosols are assumed to be externally mixed. The aerosol species that are allowed to have hygroscopic growth are sulfate, sea-salt, and organics. The sulfate and sea-salt are treated as pure (NH₄)₂SO₄ and NaCl, respectively. The organic aerosol is considered to be a mixture of four soluble compounds namely malic acid (48% by mass), citric acid (22%), glucose (4.8%), and fructose (4.7%), and a generic insoluble species (20.5%). All the species are prescribed with the same size distribution, comprising of two lognormal modes ($N_1:N_2 = 17:3$, $D_{g,1} = 0.01 \mu\text{m}$, $\sigma_1 = 1.6$, $D_{g,2} = 0.07 \mu\text{m}$, $\sigma_2 = 2.0$; where N is the number concentrations, D_g is the median diameters, and σ is standard deviations of the two modes (Whitby, 1978), which is resolved using 40 logarithmically spaced equal size bins. Dust and black carbon are not assumed to be CCN, though sulfate and BC are internally mixed for the purpose of radiative calculations. The ice droplet number concentration is prescribed and not a function of aerosol.

In this study, the model has been run with the prescribed climatological annual cycle of SST and sea-ice conditions. The climatologies of the aforementioned boundary conditions are derived using the results of GFDL's coupled model (CM4) integration's 30-year window in the PI control configuration (see RFMIP protocol in Pincus et al. (2015)). With these climatological SST and sea-ice fields, the model is run for 30 years for each of the experiments. This period is estimated to be sufficient for the computation of ERF using the fixed SST technique (P. M. Forster et al., 2016).

2.2. Data-Used

We compared our model simulated aerosol optical depth (AOD) with that derived from the collection 6 level 3 MODIS (Moderate Resolution Imaging Spectroradiometer; Levy et al., 2007) and MISR (Multiangle Imaging

Table 1
The Different Configurations in Which the GFDL AM4 Model is Run

Simulation	Aerosol species that are active in ARI	Aerosol species that are active in ACI
PD_PD_PI	S,BC,OC,D,SS	S,OC,SS
PI_PI_PI	S,BC,OC,D,SS	S,OC,SS
PI_PD_PI	S,BC,OC,D,SS	S,OC,SS
PD_PI_PI	S,BC,OC,D,SS	S,OC,SS
0_PD_PI	OC,D,SS	OC, SS
0_PI_PI	OC,D,SS	OC, SS
PD_0_PI	S,BC,D,SS	S,SS
PI_0_PI	S,BC,D,SS	S,SS
PD_0_0	S,BC	S
PI_0_0	S,BC	S
PD_PD_PI_no-SBC-ARI	OC,D,SS	S,OC,SS
PI_PI_PI_no-SBC-ARI	OC,D,SS	S,OC,SS
PD_PD_PI_no-S-ACI	S,BC,OC,D,SS	OC,SS
PI_PI_PI_no-S-ACI	S,BC,OC,D,SS	OC,SS

Note. The simulations are named in the following manner: “Emission level of sulfate-BC”_“Emission level of organic carbon”_“Emission conditions of dust and sea-salt.” The acronyms have the following meanings: PD, present-day; PI, preindustrial; 0, complete absence of the species; S, sulfate; BC, black carbon; OC, organic carbon; D, mineral dust; SS, sea-salt. A few additional runs are named by adding their specifics to the actual name of the experiment, e.g., no-SBC-ARI = sulfate-BC species are not active in aerosol-radiation interactions, similarly for no-S-ACI, where ACI means aerosol-cloud interactions.

Spectroradiometer; Kahn et al., 2005a) satellite AOD products. These data sets have also been previously utilized for evaluation of GFDL models (e.g., Hozowitz et al., 2020; Paulot et al., 2018; Zhao et al., 2018a, 2018b). The MODIS AOD is estimated to have a maximum uncertainty of $\pm 0.05 \pm 0.15 \times \text{AOD}$ (Levy et al., 2010), while that for MISR AOD is ± 0.05 or $0.2 \times \text{AOD}$ (Kahn et al., 2010). For MODIS AOD values, we utilized the mean of several level 3 products, including AOD at 550 nm from the TERRA satellite, AOD at 550 nm from the Aqua satellite, and Deep Blue AOD from the Aqua satellite (please note that Deep Blue AOD from TERRA was not available for the simulation periods). For the MISR satellite, we used the level 3 product of AOD at 555 nm from the TERRA satellite. The MODIS AOD data has a horizontal resolution of $1^\circ \times 1^\circ$, whereas the MISR data has a spatial resolution of $0.5^\circ \times 0.5^\circ$. The data sets were regridded to the model’s horizontal resolution for better comparison. To avoid any sampling bias between the model and observations, the model evaluation is done only for those pixels where the data from both MODIS and MISR exist. This explicitly avoids the analysis over cloudy pixels.

2.3. ERF of SBC Using Multiple Pathways

In this study, we calculate the 2014 ERF of SBC in GFDL AM4 with various configurations of OC, sea-salt, and dust. In some cases, we only adjust whether the cloud scheme or radiation scheme sees changes in these species. In Table 1, we list the various perturbations. Using the set of simulations (Table 1), one can obtain five different estimates of the 2014 ERF of SBC, as shown in Figure 1.

$$\text{ERF}_{\text{PI}} = R_{\text{PD_PI_PI}} - R_{\text{PI_PI_PI}} \quad (1)$$

where R is the net radiation TOA.

In this method, the ERF of SBC is computed with the emissions of other aerosol species (sea-salt, dust, and organic carbon) set to their PI levels (1850). This is particularly true for the other anthropogenic aerosols (organic carbon (OC) in this case).

$$\text{ERF}_{\text{PD}} = R_{\text{PD_PD_PI}} - R_{\text{PI_PD_PI}} \quad (2)$$

This method is similar to ERF_{PI} ; the only difference is that the emissions of OC are set to their PD levels (2014) in both of these runs (PD_PD_PI and PI_PD_PI, Table 1), unlike ERF_{PI} . The acronym subscript PD for ERF means “the other anthropogenic aerosols are set to their PD emission levels”.

$$\text{ERF}_{\text{PIN}} = R_{\text{PD_0_PI}} - R_{\text{PI_0_PI}} \quad (3)$$

This value of ERF of SBC is computed by completely removing OC from the model integration (PD_0_PI and PI_0_PI, Table 1). As the remaining aerosol species, i.e., sea-salt and dust are set to their PI emission levels we use PIN (preindustrial natural) as a suffix for the ERF computed using these model configurations.

$$\text{ERF}_{\text{Min}} = R_{\text{PD_0_0}} - R_{\text{PI_0_0}} \quad (4)$$

This ERF of SBC is computed in the complete absence of any other aerosol species. Thus for this, organic carbon, sea-salt, and mineral dust are not included (see PD_0_0 and PI_0_0 in Table 1). Thus, ERF_{Min} signifies the value of ERF of SBC, which corresponds to the minimum interference from the other aerosol species.

$$\text{ERF}_{\text{Max}} = (R_{\text{PD_PD_PI}} - R_{\text{0_PD_PI}}) - (R_{\text{PI_PI_PI}} - R_{\text{0_PI_PI}}) \quad (5)$$

In the four previous definitions (1–4), we compute the ERF as the change in net radiation at the TOA due to the change in emissions of SBC from PI to PD. In this definition, we compute the same change but in a slightly

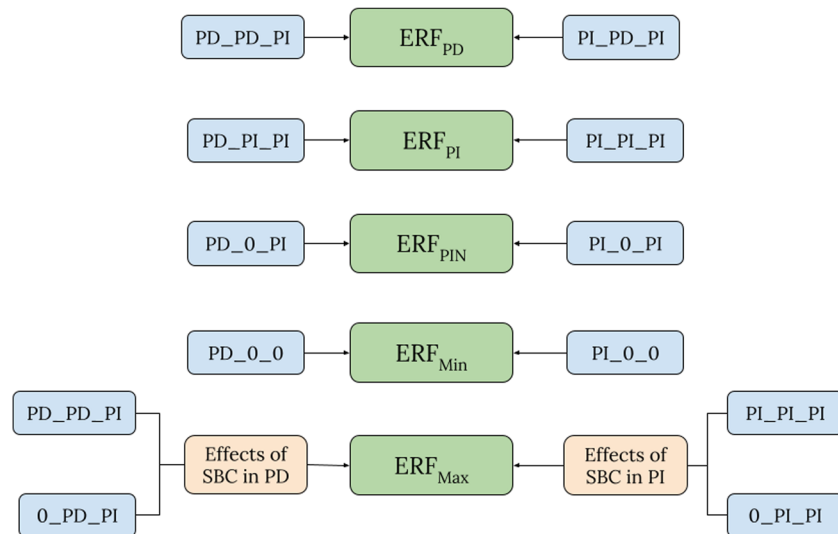


Figure 1. The five different ways in which the effective radiative forcing (ERF) of the internally mixed SBC aerosol species has been computed in this study. These ERF values mainly differ from each other in how they account for the effects of other aerosol species. The other aerosol species are most effective for ERF_{Max} formulation, while they are the least effective in ERF_{Min} formulation. The acronyms are as follows: PD, present-day; PI, preindustrial; SBC, sulfate-BC; OC, organic carbon; the subscript PD for ERF, other anthropogenic aerosols with PD conditions; the subscript PI for ERF, other anthropogenic aerosols in PI condition; PIN, the complete absence of the other anthropogenic aerosols thus allowing only the preindustrial natural aerosols to exist. Please refer to Section 2 and Table 1 for an explanation of the different configurations in which the model has been run.

different manner. We first compute the change in TOA radiation due to the inclusion of SBC in the model in PD and PI conditions (first and second term in parentheses in expression 5). The difference between these two terms gives the relative change in net radiation at TOA due to the inclusion of SBC in PD with respect to that in PI. This we define as the fifth definition of ERF. To compute the value of this ERF, we carry out AM4 simulations excluding SBC from aerosol-radiation and sulfate from ACI in PD (0_PD_PI) and PI (0_PI_PI) conditions (see Table 1 for the details). Due to the nonlinear relationship between aerosol number concentration and cloud droplet number concentration (Carslaw et al., 2013), the complete removal of sulfate from ACI, allows the other hygroscopic aerosols have enhanced (maximum possible) effects than what they would have had in the presence of sulfate. In other words, in the absence of sulfate, the other hygroscopic aerosols stand up and try to make up for the absent sulfate, in ACI. Due to this nonlinearity, the computed effects of sulfate in ACI seem lower than their true potential. Thus, this method of computing ERF of SBC is the one in which SBC (in fact, sulfate) has the least possible and the other aerosol species have the maximum possible impact in ACI. Thus, we name this ERF as ERF_{Max} , where the other aerosols have their maximum possible effects (hence Max). This value of ERF represents a lower bound for ERF of SBC.

Figure 1 describes the aforementioned five ERFs of SBC, and Table 1 describes the different configurations in which the model has been run, to compute these ERF values. It may be noted that all these runs are carried out for 30 years with the prescription of PI climatological SST and sea-ice conditions from the coupled version of the GFDL model. Note that the model is run with the same anthropogenic emissions, SST and sea-ice forcing for 30 years in order to compute the ERF following the RFMIP protocol. As can be noted from expressions 1 to 5, the five ERFs of SBC mainly differ in how they incorporate the influence of the other aerosol species (organic carbon, sea-salt, and mineral dust). Thus, with the help of these simulations and our different ERF values, we investigate how the abundance of other aerosol species controls the ERF of SBC.

2.4. Decomposition of ERF Into Its Characteristic Components

According to the framework suggested in Ghan (2013), ERF can be broken down into three radiative components, which separate the direct and indirect effects of aerosol-radiation forcing. This technique uses a double call to

the radiative transfer scheme with and without aerosol/or clouds included. Following the framework, ERF could be broken down as

$$\text{ERF} = (\text{ERF} - \text{ERF}_{\text{cln}}) + (\text{ERF}_{\text{cln}} - \text{ERF}_{\text{clr,cln}}) + \text{ERF}_{\text{clr,cln}} \quad (6)$$

We further break this down as follows:

$$\text{ERF} = \{(\text{ERF}_{\text{clr}} - \text{ERF}_{\text{clr,cln}}) + [(\text{ERF} - \text{ERF}_{\text{clr}}) - (\text{ERF}_{\text{cln}} - \text{ERF}_{\text{clr,cln}})]\} + (\text{ERF}_{\text{cln}} - \text{ERF}_{\text{clr,cln}}) + \text{ERF}_{\text{clr,cln}} \quad (7)$$

Thus,

$$\text{ERF} = \{\text{DRF}_{\text{clr}} + \text{CRF}_{\text{ari}}\} + \text{CRF}_{\text{cln}} + \text{AF} \quad (8)$$

All the ERF values are computed as ΔR (Δ stands for the difference between PD and PI states) where “clr” represents cloud-free (clear-sky) conditions, “cln” represents aerosol-free (clean-sky) radiation calculations, while “clr,cln” stands for aerosol and cloud-free radiation calculations. The acronyms in (8) have the following meanings:

$\text{DRF}_{\text{clr}} = (\text{ERF}_{\text{clr}} - \text{ERF}_{\text{clr,cln}}) \equiv$ ERF associated with the direct radiative effects of aerosols in clear-sky conditions

$\text{CRF}_{\text{ari}} = [(\text{ERF} - \text{ERF}_{\text{clr}}) - (\text{ERF}_{\text{cln}} - \text{ERF}_{\text{clr,cln}})] \equiv$ the difference between the cloud radiative forcing in “all-sky” conditions and that in “clean-sky” conditions. So, this term signifies the change in the cloud radiative effect due to direct ARI. In other words, this term also signifies the effects of clouds on DRF_{clr}

$\text{CRF}_{\text{cln}} = (\text{ERF}_{\text{cln}} - \text{ERF}_{\text{clr,cln}}) \equiv$ cloud radiative forcing in “clean-sky” conditions

$\text{AF} = \text{ERF}_{\text{clr,cln}} \equiv$ ERF associated with noncloud-nonaerosol features (e.g., surface albedo)

Thus, it can be seen that we have slightly modified the decomposition of ERF suggested by Ghan (2013). We break the direct RF of aerosols into their clear-sky and cloud radiative effect components. In this study, we have used expressions 7 and 8 to decompose the ERF of SBC.

3. Results and Discussion

3.1. Comparison of Model-Simulated Aerosol Optical Depth With the Satellite Products

Since we are studying ERF of the PD aerosols, we need to determine how realistic is the distribution of PD aerosols in the model. We compare the model simulated AOD against observations. Zhao et al. (2018a), show that AM4 simulated AOD (at 550-nm wavelength) agrees reasonably well with the AERONET measurements. We briefly revisit such model-observation comparisons for the simulated AOD (at 550 nm) in AM4 (Figure 2). We compare the area-averaged AOD in AM4 over the different polluted regions of the world with that retrieved by MODIS (Levy et al., 2007) and MISR (Kahn et al., 2005b) satellite instruments. The comparisons are made for the year 2014. While the satellite AOD products themselves differ from each other, with MISR AOD being the lower bound, the model simulated AOD indicates a reasonably good agreement (Figure 2). As the focus of our work is to understand ERF of individual aerosol species (SBC) and the impacts of other aerosol, we speciate the composite AOD into the individual species. Note that while sulfate and black carbon are treated individually, the optical properties (extinction coefficient, single-scattering albedo, and asymmetry parameter) for sulfate and hydrophilic black carbon are assigned by assuming their internal mixture, as mentioned previously. Therefore, we combine sulfate and BC AOD and assign that to the internally mixed SBC aerosol species. While the natural aerosols (sea-salt and mineral dust) contribute at par with the anthropogenic aerosols on the global as well as the northern hemispheric mean basis (Figure 2), over the polluted regions their anthropogenic counterparts (SBC and OC) dominate the scene. Especially over the Asian pollution hot-spots such as East China and India, SBC together contribute to approximately one-half to two-thirds of the total AOD in AM4, across the four seasons. In the face of this domination by SBC in these regions, it is interesting to investigate the extent the conditions of other aerosol species matter for the computation of the ERF of SBC.

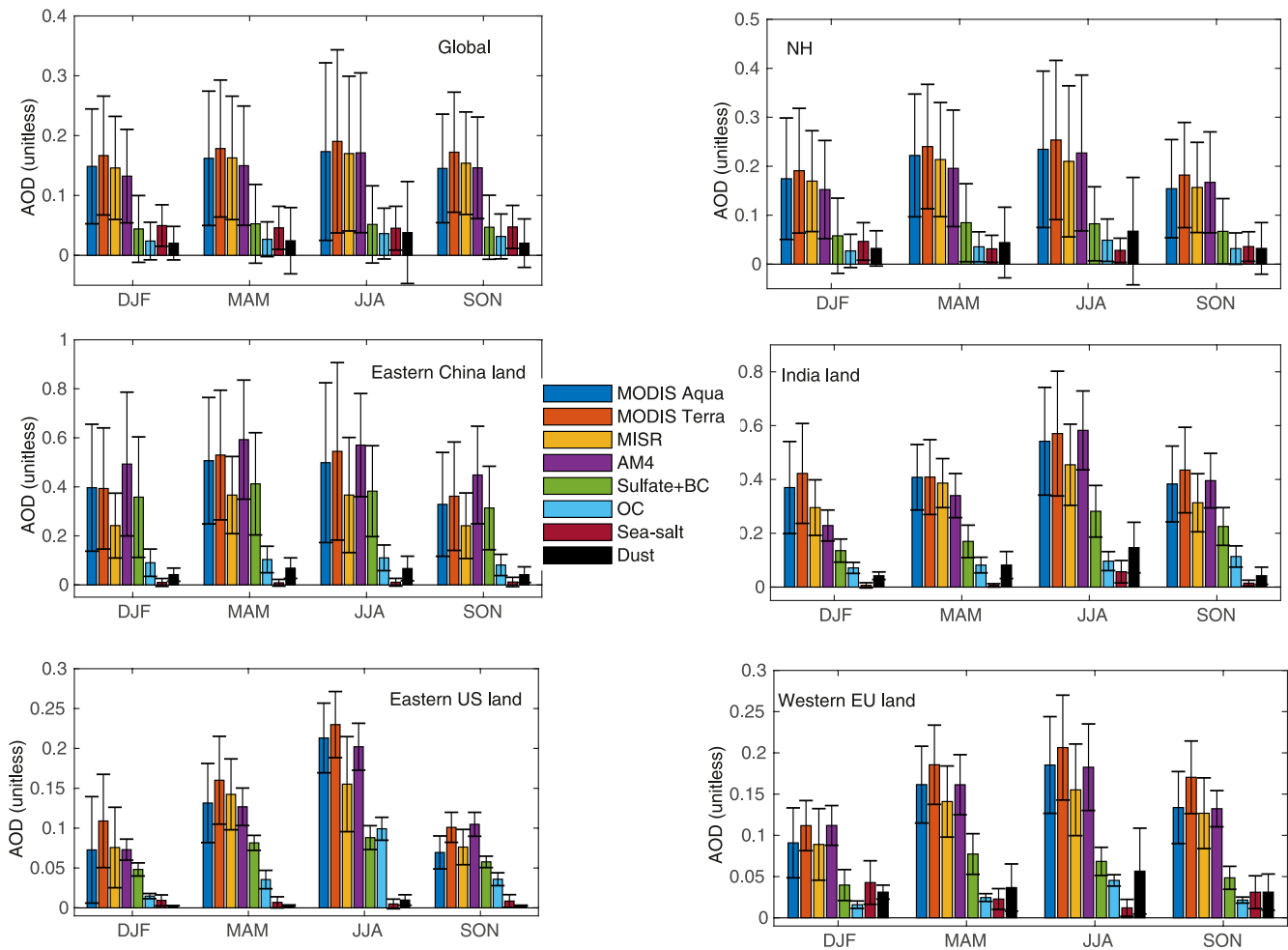


Figure 2. Comparison of AM4 simulated aerosol optical depth (AOD) (at 550 nm) with that retrieved by satellite instruments namely MODIS and MISR onboard TERRA and Aqua satellites. The comparisons are made for the polluted land regions of East China (100°E:130°E, 20°N:45°N), India (65°E:95°E, 5°N:30°N), Eastern United States (260°E:290°E, 30°N:50°N), and Western Europe (15°W:20°E, 35°N:60°N). The model-simulated AOD has been further broken down into the different aerosol species. The colored bars represent the area-averaged values, while the thin bars stand for ± 1 standard deviation about the mean. The model simulations done in the “PD_PD_PI” configuration are used to compare the satellite observations for the year 2014. The y-axis for “India land” box represents AOD (unitless).

3.2. Effective Radiative Forcing of SBC: Role of Other Aerosol Species

The ERF of the SBC aerosol species is computed by following the five different configurations of OC, dust, and sea-salt detailed in Section 2.

Figure 3 shows the spatial distribution of the five 2014 ERFs of SBC. The spatial pattern of ERF remains largely similar across the five methods, with maximum negative (scattering) ERF over the polluted regions like East China and India and net absorbing effect mainly over the regions with high surface albedo (deserts of Sahara and India). The magnitude of the ERF, however, is seen to change significantly across some of the methods. While maximizing the impact of other aerosol (ERF_{Max}) or changing the value of OC from 1850 (ERF_{PI}) to 2014 (ERF_{PD}) have a minimal impact and present comparable ERF values, the last two methods, which remove OC (ERF_{PIN}) or remove OC, sea-salt, and dust aerosol (ERF_{Min}) depict substantially high (more negative) and statistically different values.

To further highlight the difference in the methods, we compute area-averaged 2014 SBC ERF for the entire globe, the northern hemisphere, and landmasses of heavily polluted regions like East China, India, Eastern United States of America (EUS), and Western Europe (WEU), using all the five methods, in Figure 4.

In contrast, over the regional hot spots, the magnitude of ERF for SBC strongly depends on whether the 1850 or 2014 emission levels for OC are used. In general, the stronger the influence or abundance of the other aerosol species, the lower the ERF of SBC, i.e., ERF_{Max} is the minimum, while ERF_{Min} is the maximum

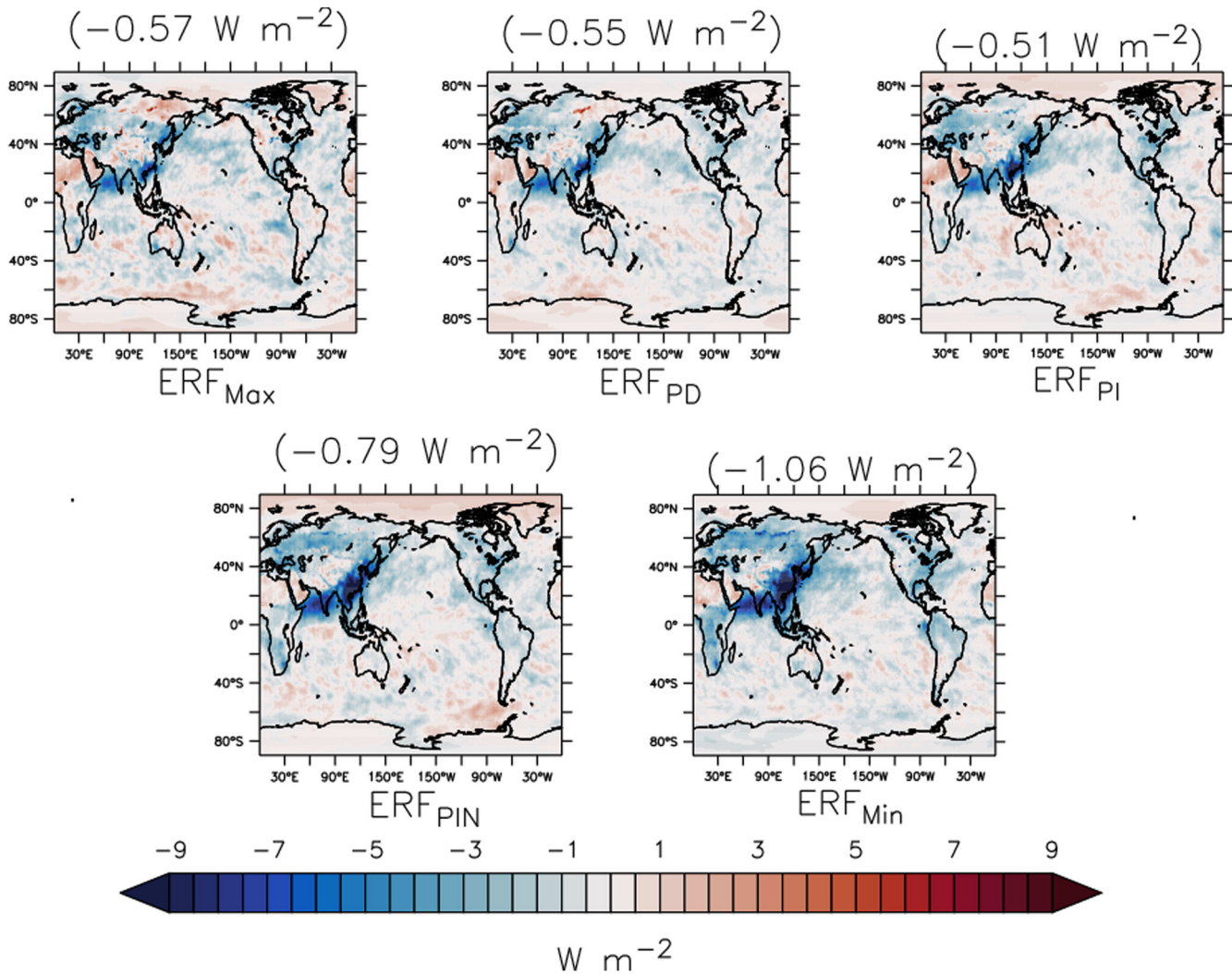


Figure 3. The 2014 effective radiative forcing (ERF) of the sulfate-black carbon (SBC) aerosol species in GFDL AM4 model, calculated using five different definitions. These ERF values mainly differ from each other in the manner in which they account for the effects of other aerosol species (OC, sea-salt, and mineral dust in this case). The other aerosol species are most effective for ERF_{Max} formulations, while they are least effective in ERF_{Min} formulation. Refer to Section 2, Figure 1, and Table 1, for the different definitions of ERF of SBC and the model simulations utilized for those. The negative values indicate net cooling. The numbers in the parentheses indicate the global mean values of ERF of SBC.

among the five ERFs of SBC (Figure 4). There is a systematic increase in the magnitude of ERF of SBC with the reduction in the concentration or influence of the other aerosol species. Over the landmass of East China, ERF_{Max} is almost 60% of ERF_{PI} value. The ERF_{PD} and ERF_{PI} , which simply differ from each other in terms of the conditions of OC aerosols, still diverge from each other by $\sim 25\%$ – 30% . In Figures S1 and S2 in Supporting Information S1, we decompose the total ERF into its shortwave and longwave components. Table S1 in Supporting Information S1 presents the analysis of regional SW and LW ERF values following the five different configurations.

Given the importance of the other aerosol species for the computation of ERF of SBC, we show the AOD associated with them in the aforementioned different formulations employed in Figure 5. The corresponding AOD decreases from ERF_{PD} to ERF_{PI} and further to ERF_{PIN} , especially for polluted regions like East China and India. However, the regions like the Eastern US and the Western EU show smaller differences in the other aerosols' optical depth in PD from PI. The corresponding AOD for ERF_{Min} configuration is zero. On the other hand, due to how ERF_{Max} is computed, it is not possible to assign a single value of such AOD to it. Nevertheless, there is a strict dependence of the ERF of SBC (Figure 4) on the magnitude of the AOD associated with the other aerosol species. However, this control may come from not only the direct effects but also the indirect effects. We explore this in the next section.

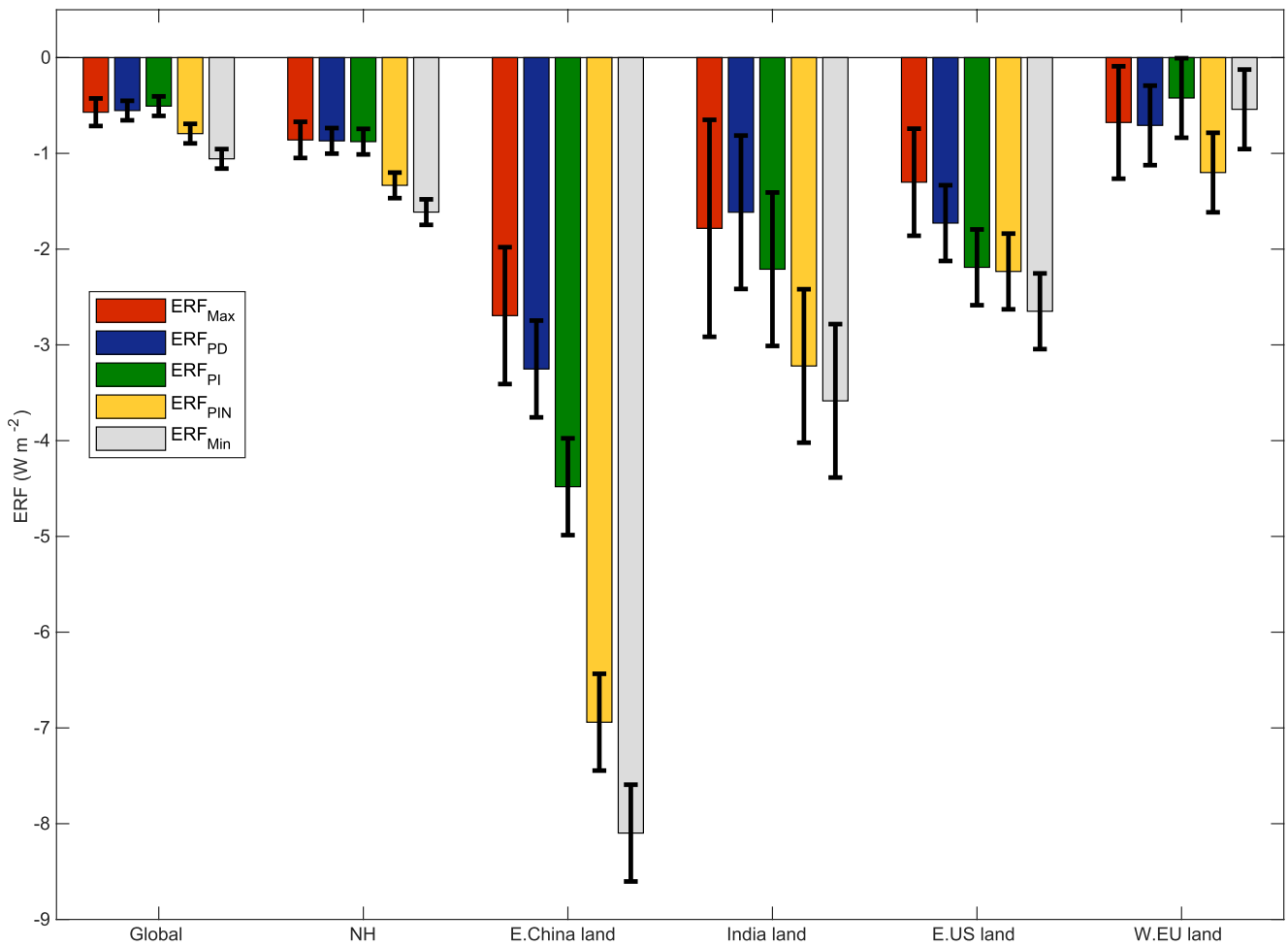


Figure 4. The 2014 sulfate-black carbon effective radiative forcing in the GFDL AM4 model, averaged over the different polluted regions of the globe. East China = 100°E:130°E, 20°N:45°N; India = 65°E:95°E, 5°N:30°N; Eastern US = 260°E:290°E, 30°N:50°N; and Western EU = 15°W:20°E, 45°N:60°N. The negative values indicate net cooling. The uncertainty bars represent ± 1 standard deviation from the mean.

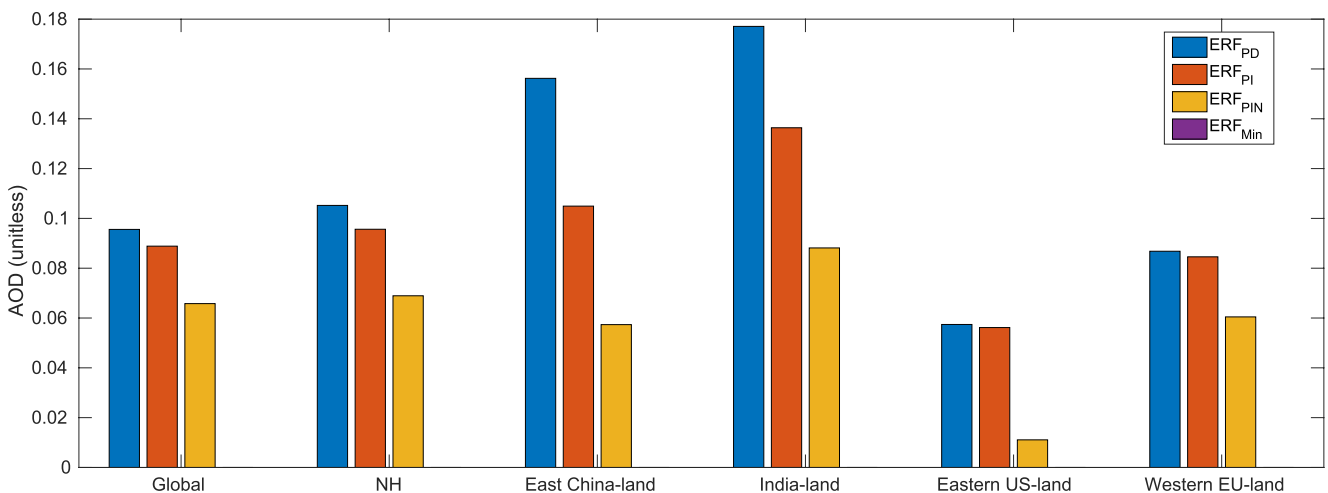


Figure 5. The magnitude of the regional-mean optical depth of the other aerosol species in the different formulations of effective radiative forcing mentioned in Figure 1 and Section 3.2.

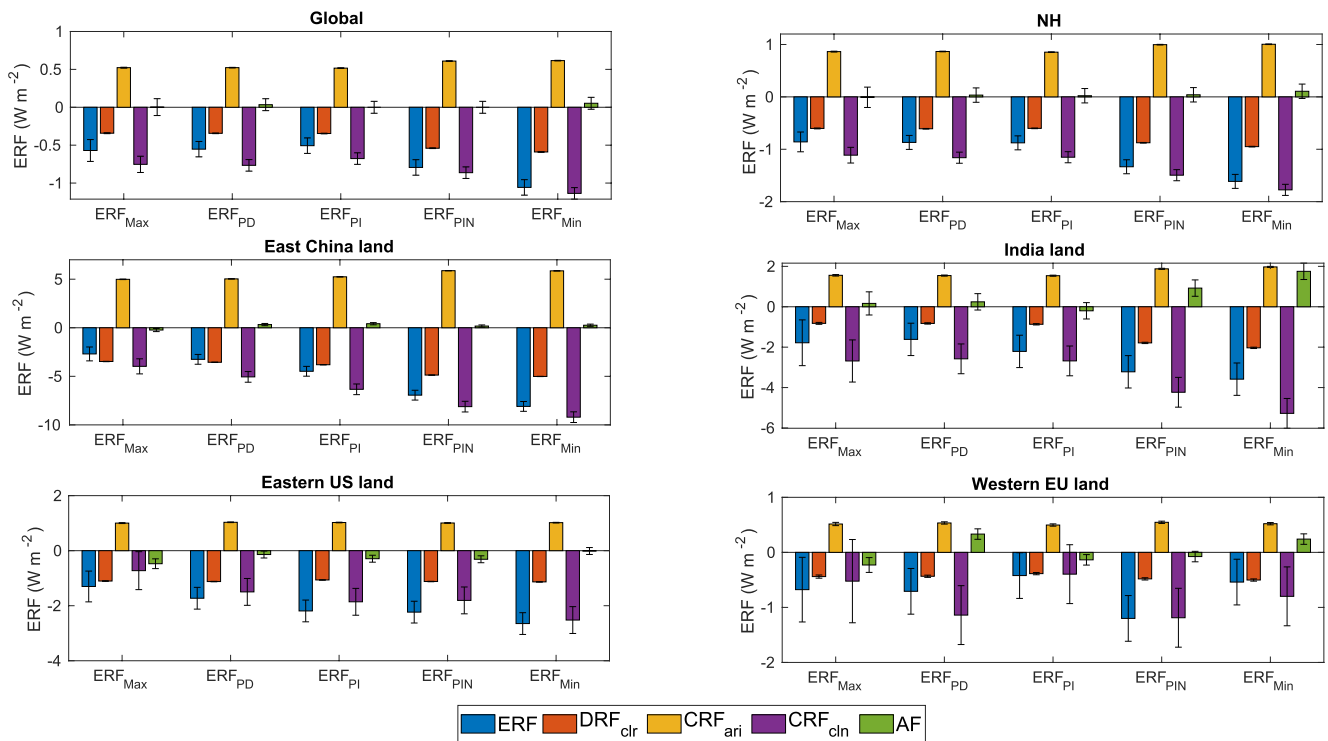


Figure 6. Decomposition of five 2014 sulfate-black carbon effective radiative forcings into their characteristic components (expression 8) over different regions of the world. The positive values indicate net warming. The uncertainty bars represent ± 1 standard deviation from the mean.

3.3. Decomposition of ERF of SBC Into Its Characteristics Components

The previous section shows that the 2014 ERF of SBC depends upon conditions or abundance of other aerosol species. To understand the physical processes that predominantly bring about such a dependence, we first decompose the five ERFs of SBC into their characteristic components to reveal the causes. In Figure 6, we decompose the total ERF of SBC shown in Figure 4 into DRF_{clr} , CRF_{ari} , CRF_{cln} , and AF components as discussed in Equations 7 and 8, with each bar in Figure 4 split into the four components. As mentioned previously, our framework explicitly reveals the modulation of the ERF of aerosols by clouds. The DRF_{clr} component (Figure 6) is seen to be consistently negative (i.e., of scattering nature) across the chosen regions. On the other hand, the clouds tend to make aerosol direct RF more absorbing (CRF_{ari} component, Figure 6) across the methods and in all the regions. The third and major component of the ERF budget is CRF_{cln} , i.e., the cloud RF in clean conditions. It is this component that mainly varies across the five methods and thus depends strongly on the conditions (abundance) of other aerosols. As explained previously, ERF_{Max} (ERF_{Min}) has the maximum (minimum) influence of the other aerosol species. The higher the abundance or influence of other aerosol species, the lesser the magnitude of the CRF_{cln} component. Thus, it is the CRF_{cln} component that imparts the dependence on the conditions of other aerosols, to ERF. Thus, apart from CRF_{cln} , all other components are seen to be relatively independent of the choice of method for the ERF computation. The CRF_{cln} component has been shown to be related to aerosol-cloud microphysical interactions (Ghan, 2013). In the next section, we conduct additional model experiments to confirm this association.

3.4. The Physical Processes Involved in the CRF_{cln} Component of ERF of SBC

To confirm the association of ACI to the CRF_{cln} component of the ERF of SBC, we carry out a few more model experiments. We split the total ERF of SBC into that due to ARI (ERF_{ARI}) and that due to ACI (ERF_{ACI}). We use ERF_{Max} for this exercise and split that into ERF_{ARI} and ERF_{ACI} . Making use of the “PD_PD_PI_no-SBC-ARI” and “PI_PI_PI_no-SBC-ARI” (i.e., simulations in which no SBC is seen by the radiation scheme) and “PD_PD_PI_no-S-ACI” and “PI_PI_PI_no-S-ACI” (i.e., simulations in which no sulfate is seen by the aerosol-cloud microphysics scheme) simulations along with the control simulations (PD_PD_PI and PI_PI_PI)

listed in Table 1, ERF due to ARI of SBC and that due to ACI of SBC can be computed in the same manner as ERF_{Max} .

$$ERF_{ARI}^1 = (R_{PD_PD_PI} - R_{PD_PD_PI_no-SBC-ARI}) - (R_{PI_PI_PI} - R_{PI_PI_PI_no-SBC-ARI}) \quad (9)$$

$$ERF_{ACI}^1 = (R_{PD_PD_PI} - R_{PD_PD_PI_no-S-ACI}) - (R_{PI_PI_PI} - R_{PI_PI_PI_no-S-ACI}) \quad (10)$$

Here, superscript 1 refers to one way of computing ERF_{ACI} and ERF_{ARI} .

Similar to the methodology followed in computing ERF_{ACI} in the IPCC Assessment Report 5 (AR5) (Myhre et al., 2013), ERF_{ARI} and ERF_{ACI} can be alternatively computed as the residual term from Equation 9 or Equation 10 subtracted from ERF_{Max} (Equation 5)

$$ERF_{ARI}^2 = ERF_{Max} - ERF_{ACI}^1 \quad (11)$$

$$ERF_{ACI}^2 = ERF_{Max} - ERF_{ARI}^1 \quad (12)$$

Here, superscript 2 refers to this alternate way of computing ERF_{ACI} and ERF_{ARI} .

We make use of both these definitions and compute ERF_{ARI} and ERF_{ACI} as the mean of both of them; thus

$$ERF_{ARI} = (ERF_{ARI}^1 + ERF_{ARI}^2)/2 \text{ and } ERF_{ACI} = (ERF_{ACI}^1 + ERF_{ACI}^2)/2 \quad (13)$$

Upon computing ERF_{ARI} and ERF_{ACI} , we further decompose those into the same four components from Figure 6 using the methodology discussed in Equations 7 and 8. This decomposition would also help explain the contribution of ARI and ACI to each component of ERF of SBC, specifically to the CRF_{clin} component. In Figure 6, we decompose ERF_{ARI} and ERF_{ACI} into the aforementioned four characteristic components.

The first set of bars in all the panels of Figure 7 is the same as that ERF_{Max} in Figure 6. These bars represent the decomposition of ERF_{Max} into the four components (Equations 7 and 8). These bars are further decomposed into the ARI (second set of bars in Figure 7) and ACI (third set of bars in Figure 7) shares. It can be seen that the first two and the last components of ERF of SBC can be primarily attributed to ARI of SBC (bars from set 2, Figure 6). The third component, i.e., CRF_{clin} (from the first set of bars, Figure 7), on the other hand, can be mainly attributed to ACI of SBC (bars from set 3, Figure 7). Nevertheless, ARI of SBC also has a nonnegligible contribution (bar from set 2, Figure 7), which would arise due to rapid adjustments to the ARI of PD SBC. However, in general, the ACI mainly contribute to CRF_{clin} . Thus, our experiments and the corresponding analysis confirm the result from Ghan's decomposition (Ghan, 2013) that the CRF_{clin} component is mainly related to ACI. As shown in Figure 6, the CRF_{clin} primarily imparts dependence on the conditions of other aerosol species to the ERF of SBC. Thus, the ACI are the ones that impart this dependence to the CRF_{clin} component and, thus, to the ERF of SBC. The strength of ACI does depend upon the abundance of the other aerosol concentrations. The higher the background aerosol concentration, the lesser is the sensitivity of the climate to the indirect effects of anthropogenic aerosol species (Carslaw et al., 2013). Thus, the dependence of ERF of SBC on the background state of other aerosols is mainly attributable to ACI.

The five configurations mainly differ from each other in terms of the availability of the aerosols other than SBC in ARI and ACI processes (Table 1). We show that the ARI of SBC does not show a large dependence on the availability of the other aerosols; on the other hand, the ACI does show a much greater dependence on the availability of the other aerosols (Figure 7). For ACI, the potential of any hydrophilic species would not only depend on its own physical and chemical properties but also on the availability and the physiochemical properties of the other hygroscopic species in the environment (see Figure 3 of Carslaw et al. (2013)). Note the strong sublinear relationship between cloud albedo and available aerosol concentrations (Figure 3d of Carslaw et al. (2013)). It clearly signifies that the cloud albedo varies more strongly with the available aerosol concentrations when the concentrations are lesser. As the aerosol concentrations increase, the sensitivity of cloud albedo to those drops down rapidly. This relationship between cloud albedo and aerosols is the basis for differences that we notice in ACI-induced ERF in those five different configurations. Therefore, in the ERF_{Min} configuration where there are no other aerosols present in the model apart from SBC, the cloud albedo is the most sensitive to SBC and thus, the ERF associated with ACI of SBC is the highest. As one systematically starts to increase the available concentrations of aerosol from ERF_{Min} to ERF_{PIN} , to ERF_{PI} , and finally to ERF_{PD} , the sensitivity of cloud albedo to SBC drops down (see Figure

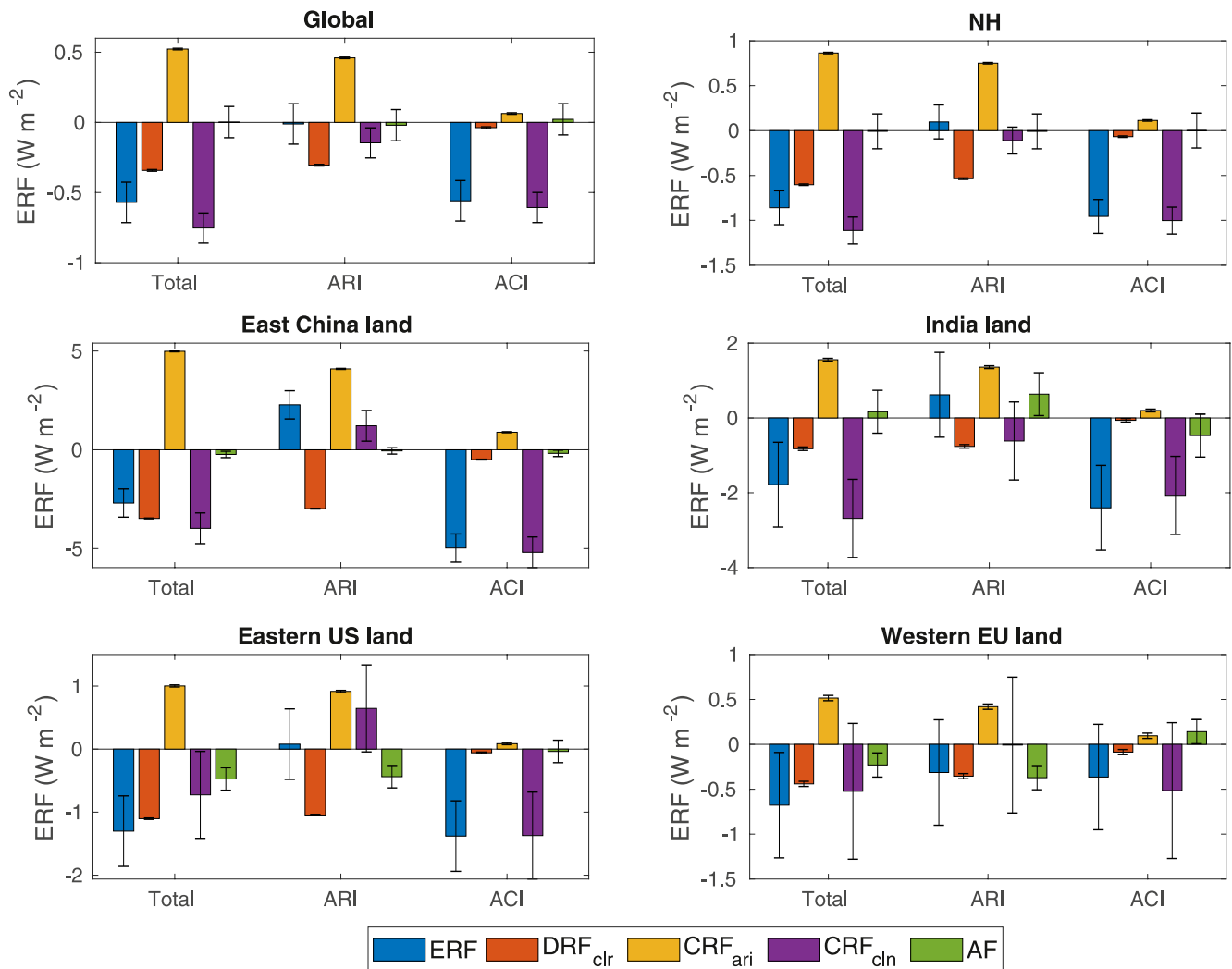


Figure 7. Decomposition of ERF_{Max} of sulfate-black carbon into the aerosol-radiation interaction and aerosol-cloud interaction components and further decomposition of those into their characteristic components following expression 8, over the different regions of the globe. The positive values indicate net warming. The uncertainty bars represent ± 1 standard deviation from the mean.

3d from Carslaw et al. (2013)), and hence the ERF associated with ACI of SBC also drops down. The ERF_{Max} is a unique configuration in which we allow the “other” aerosols to have their maximum impact (see Section 2); this further results in an even smaller ERF of SBC. Thus, in this manner, the sublinear relationship between cloud albedo and aerosol concentrations turns out to be the cause behind the differences in the ERF of SBC computed using the five different configurations considered in this study. All the components of ERF that are mainly related to ARI of SBC are relatively independent of the state of other aerosol species. Moreover, the total ERF due to ARI of SBC (second set of bars, Figure 6) turns out to be very small as a result of cancellation between its different components. As a result, it is the ACI that dominates the magnitude and sign of total ERF of SBC.

Similar to SBC, the ERF of any other anthropogenic aerosols like OC, nitrate, etc., would depend not only on their own concentrations in the PI conditions but also the concentration of the other species as illustrated in this study. Our study highlights the role played by ACI in imparting such dependence on the conditions of other aerosols for the computed ERF of the species of interest. While the study reveals the cause of this dependence, the magnitude of the dependence would vary across different models. More precisely, the magnitude depends on the strength of the aerosol-indirect effects prescribed in the models. This, in turn, also depends upon the simulated meteorological parameters, e.g., specific humidity, temperature, rainfall, boundary layer turbulence, winds, and the aerosol properties, e.g., the mass concentration, state of mixing of aerosols, assigned hygroscopicity values, parameterization options for ACI. The analysis and results here suggest that model sensitivity to the influences

of the other aerosols on the composite SBC ERF be explored across different models (e.g., CMIP models) to estimate the intermodel uncertainty. To compute the ERF of any individual aerosol species, it would be practical to keep the other anthropogenic aerosols to the PD state, as these species would also vary with the anthropogenic species of interest owing to coemission.

Using a modified version of Ghan's technique (Ghan, 2013) of decomposition of aerosol forcing, we provide a comprehensive look at the aerosol ERF and the interactions of clouds with them. With this modified decomposition, the absorption enhancement of aerosols by clouds is revealed. However, what causes clouds to impart the absorption signature to the broadly scattering aerosol species has not been explored here. The technique employed here does not need any new variables to be generated. It uses the same variables in a more comprehensive formulation and diagnostics related to aerosol forcing.

4. Conclusions

With the motivation to investigate the role played by other aerosol species in the computation of species-wise ERF for aerosols, this study computed the PI to PD ERF of the internally mixed SBC aerosol species using the GFDL AM4. Model experiments show that the ERF of SBC can be calculated in at least five different configurations (details can be found in Section 2) by varying the emission levels of the other aerosols species (i.e., organic carbon, sea-salt, and mineral dust). Significantly different values of ERF of SBC are found across these five methods, especially over the regional hot spots of aerosols. The main conclusions from the study could be summarized as follows:

1. The global mean ERF of the SBC aerosol species in the GFDL AM4 model ranges between -0.51 ± 0.1 and $-1.06 \pm 0.1 \text{ W m}^{-2}$ depending upon the choice of the abundance of the other aerosol species. While two of the five combinations exclude one or more aerosol species from the ERF computation (which is somewhat unrealistic but included here for completeness), the other three combinations are more realistic and employed widely in the literature.
2. Two of the realistic configurations involve setting the anthropogenic emissions of organic carbon aerosol species to the PI (1850) or the PD (2014) conditions. It is found that over polluted regions, e.g., eastern China, the ERF of SBC computed using those two methods differ by $\sim 37\%$, suggesting that the choice of the emissions of organic carbon aerosol species tightly controls the regional-mean ERF of SBC. The higher the emissions or the abundance of the other aerosol species, the lower is the ERF of SBC.
3. On further decomposing the ERF into its characteristic components, using a slightly modified version of the Ghan (2013) formulation, the ERF associated with ACI (CRF_{cln}) turns out to be the component that imparts a high dependence on the conditions of the other aerosol species. The higher the concentration of those, the lower is the value of CRF_{cln} .
4. Novel model experiments confirm the association of the CRF_{cln} component to the ACI. Our analysis suggests that a major portion of the CRF_{cln} component is associated with the ACI (confirming the Ghan decomposition); however, the ARI also provide a nonnegligible contribution to the CRF_{cln} component through the fast-tropospheric adjustments.
5. The forcing associated with ARI is relatively small due to the cancellation of direct RF of aerosols in clear-sky and the absorption enhancement of aerosols by clouds.
6. The technique here explicitly breaks down the direct radiative effects of aerosols in clear-sky conditions and the effects of clouds. The analyses and results suggest that this technique can be utilized for future aerosol-forcing-related diagnostics.

In summary, our study suggests that for emissions-based aerosol forcing estimates, the choice of emissions of other aerosol species does affect the ERF of the species of interest, especially over the regional aerosol hot-spots. The same would hold true even for concentration-based forcing estimates. This dependence mainly comes from the dependence of the ACI on the abundance of the other aerosols.

Conflict of Interest

The authors declare no conflicts of interest relevant to this study.

Data Availability Statement

The data from the satellite products (MODIS and MISR) have been downloaded from <https://giovanni.gsfc.nasa.gov/giovanni/>. The data on which this article is based are available in Govardhan et al. (2022).

Acknowledgments

The authors would like to thank Jing Feng and Vaishali Naik for their constructive comments, which improved the state of the manuscript. We would also like to thank the three anonymous reviewers for very useful comments/suggestions on the manuscript.

References

- Abel, S. J., Haywood, J. M., Highwood, E. J., Li, J., & Buseck, P. R. (2003). Evolution of biomass burning aerosol properties from an agricultural fire in southern Africa. *Geophysical Research Letters*, *30*(15), 1783. <https://doi.org/10.1029/2003GL017342>
- Andrews, T. (2014). Using an AGCM to diagnose historical effective radiative forcing and mechanisms of recent decadal climate change. *Journal of Climate*, *27*(3), 1193–1209. <https://doi.org/10.1175/jcli-d-13-00336.1>
- Bondietti, E. A., & Papastefanou, C. (1993). Estimates of residence times of sulfate aerosols in ambient air. *Science of the Total Environment*, *136*(1–2), 25–31. [https://doi.org/10.1016/0048-9697\(93\)90294-g](https://doi.org/10.1016/0048-9697(93)90294-g)
- Cape, J. N., Coyle, M., & Dumitrescu, P. (2012). The atmospheric lifetime of black carbon. *Atmospheric Environment*, *59*, 256–263. <https://doi.org/10.1016/j.atmosenv.2012.05.030>
- Carlsaw, K. S., Gordon, H., Hamilton, D. S., Johnson, J. S., Regayre, L. A., Yoshioka, M., & Pringle, K. J. (2017). Aerosols in the pre-industrial atmosphere. *Current Climate Change Reports*, *3*(1), 1–15. <https://doi.org/10.1007/s40641-017-0061-2>
- Carlsaw, K. S., Lee, L. A., Reddington, C. L., Pringle, K. J., Rap, A., Forster, P. M., et al. (2013). Large contribution of natural aerosols to uncertainty in indirect forcing. *Nature*, *503*(7474), 67–71. <https://doi.org/10.1038/nature12674>
- Chung, E.-S., & Soden, B. J. (2015). An assessment of methods for computing radiative forcing in climate models. *Environmental Research Letters*, *10*(7), 074004. <https://doi.org/10.1088/1748-9326/10/7/074004>
- Donner, L. J., Wyman, B. L., Hemler, R. S., Horowitz, L. W., Ming, Y., Zhao, M., et al. (2011). The dynamical core, physical parameterizations, and basic simulation characteristics of the atmospheric component AM3 of the GFDL global coupled model CM3. *Journal of Climate*, *24*(13), 3484–3519. <https://doi.org/10.1175/2011jcli3955.1>
- Fiedler, S., Stevens, B., & Mauritsen, T. (2017). On the sensitivity of anthropogenic aerosol forcing to model-internal variability and parameterizing a Twomey effect. *Journal of Advances in Modeling Earth Systems*, *9*, 1325–1341. <https://doi.org/10.1002/2017MS000932>
- Forster, P., Storelvmo, T., Armour, K., Collins, W., Dufresne, J.-L., Frame, D., et al. (2021). The Earth's Energy budget, climate feedbacks, and climate sensitivity. In V. Masson-Delmotte, P. Zhai, A. Pirani, S. L. Connors, C. Péan, S. Berger, et al. (Eds.), *Climate change 2021: The physical science basis. Contribution of working group I to the sixth assessment report of the intergovernmental panel on climate change* (pp. 923–1054). Cambridge University Press. <https://doi.org/10.1017/9781009157896.009>
- Forster, P. M., Richardson, T., Maycock, A. C., Smith, C. J., Samsel, B. H., Myhre, G., et al. (2016). Recommendations for diagnosing effective radiative forcing from climate models for CMIP6. *Journal of Geophysical Research: Atmospheres*, *121*, 12460–12475. <https://doi.org/10.1002/2016JD025320>
- Freidenreich, S. M., & Ramaswamy, V. (1999). A new multiple-band solar radiative parameterization for general circulation models. *Journal of Geophysical Research*, *104*(D24), 31389–31409. <https://doi.org/10.1029/1999JD900456>
- Ghan, S. J. (2013). Technical note: Estimating aerosol effects on cloud radiative forcing. *Atmospheric Chemistry and Physics*, *13*(19), 9971–9974. <https://doi.org/10.5194/acp-13-9971-2013>
- Ginoux, P., Horowitz, L. W., Ramaswamy, V., Geogdzhayev, I. V., Holben, B. N., Stenchikov, G., & Tie, X. (2006). Evaluation of aerosol distribution and optical depth in the Geophysical Fluid Dynamics Laboratory coupled model CM2.1 for present climate. *Journal of Geophysical Research*, *111*, D22210. <https://doi.org/10.1029/2005JD006707>
- Govardhan, G., Paynter, D., & Ramaswamy, V. (2022). Dataset for the aerosol-ERF paper [Dataset]. Zenodo. <https://doi.org/10.5281/zenodo.7498685>
- Hamilton, D. S., Hantson, S., Scott, C. E., Kaplan, J. O., Pringle, K. J., Nieradzki, L. P., et al. (2018). Reassessment of pre-industrial fire emissions strongly affects anthropogenic aerosol forcing. *Nature Communications*, *9*(1), 3182. <https://doi.org/10.1038/s41467-018-05592-9>
- Hansen, J., Sato, M., & Ruedy, R. (1997). Radiative forcing and climate response. *Journal of Geophysical Research*, *102*(D6), 6831–6864. <https://doi.org/10.1029/96JD03436>
- Hansen, J., Sato, M., Ruedy, R., Nazarenko, L., Lacis, A., Schmidt, G. A., et al. (2005). Efficacy of climate forcings. *Journal of Geophysical Research*, *110*, D18104. <https://doi.org/10.1029/2005JD005776>
- Haywood, J. M., & Ramaswamy, V. (1998). Global sensitivity studies of the direct radiative forcing due to anthropogenic sulfate and black carbon aerosols. *Journal of Geophysical Research*, *103*(D6), 6043–6058. <https://doi.org/10.1029/97JD03426>
- Held, I. M., Guo, H., Adcroft, A., Dunne, J. P., Horowitz, L. W., Krasting, J., et al. (2019). Structure and performance of GFDL's CM4.0 climate model. *Journal of Advances in Modeling Earth Systems*, *11*, 3691–3727. <https://doi.org/10.1029/2019MS001829>
- Hess, M., Koepke, P., & Schult, I. (1998). Optical properties of aerosols and clouds: The software package OPAC. *Bulletin of the American Meteorological Society*, *79*(5), 831–844. [https://doi.org/10.1175/1520-0477\(1998\)079<0831:opoaac>2.0.co;2](https://doi.org/10.1175/1520-0477(1998)079<0831:opoaac>2.0.co;2)
- Hoesly, R. M., Smith, S. J., Feng, L., Klimont, Z., Janssens-Maenhout, G., Pitkanen, T., et al. (2018). Historical (1750–2014) anthropogenic emissions of reactive gases and aerosols from the Community Emissions Data System (CEDS). *Geoscientific Model Development*, *11*(1), 369–408. <https://doi.org/10.5194/gmd-11-369-2018>
- Horowitz, L. W., Naik, V., Paulot, F., Ginoux, P. A., Dunne, J. P., Mao, J., et al. (2020). The GFDL global atmospheric chemistry-climate model-IAM4.1: Model description and simulation characteristics. *Journal of Advances in Modeling Earth Systems*, *12*, e2019MS002032. <https://doi.org/10.1029/2019MS002032>
- Kahn, R. A., Gaitley, B. J., Garay, M. J., Diner, D. J., Eck, T. F., Smirnov, A., & Holben, B. N. (2010). Multiangle Imaging Spectroradiometer global aerosol product assessment by comparison with the Aerosol Robotic Network. *Journal of Geophysical Research*, *115*, D23209. <https://doi.org/10.1029/2010JD014601>
- Kahn, R. A., Gaitley, B. J., Martonchik, J. V., Diner, D. J., Crean, K. A., & Holben, B. (2005a). Multiangle Imaging Spectroradiometer (MISR) global aerosol optical depth validation based on 2 years of coincident Aerosol Robotic Network (AERONET) observations. *Journal of Geophysical Research*, *110*, D10S04. <https://doi.org/10.1029/2004JD004706>
- Kahn, R. A., Li, W.-H., Martonchik, J. V., Bruegge, C. J., Diner, D. J., Gaitley, B. J., et al. (2005b). MISR calibration and implications for low-light-level aerosol retrieval over dark water. *Journal of the Atmospheric Sciences*, *62*(4), 1032–1052. <https://doi.org/10.1175/JAS3390.1>
- Knutti, R., Rugenstein, M. A. A., & Hegerl, G. C. (2017). Beyond equilibrium climate sensitivity. *Nature Geoscience*, *10*(10), 727–736. <https://doi.org/10.1038/ngeo3017>

- Kretzschmar, J., Salzmann, M., Mülmenstädt, J., Boucher, O., & Quaas, J. (2017). Comment on “Rethinking the lower bound on aerosol radiative forcing”. *Journal of Climate*, *30*(16), 6579–6584. <https://doi.org/10.1175/jcli-d-16-0668.1>
- Levy, R. C., Remer, L. A., Kleidman, R. G., Mattoo, S., Ichoku, C., Kahn, R., & Eck, T. F. (2010). Global evaluation of the Collection 5 MODIS dark-target aerosol products over land. *Atmospheric Chemistry and Physics*, *10*(21), 10399–10420. <https://doi.org/10.5194/acp-10-10399-2010>
- Levy, R. C., Remer, L. A., Mattoo, S., Vermote, E. F., & Kaufman, Y. J. (2007). Second-generation operational algorithm: Retrieval of aerosol properties over land from inversion of Moderate Resolution Imaging Spectroradiometer spectral reflectance. *Journal of Geophysical Research*, *112*, D13211. <https://doi.org/10.1029/2006JD007811>
- Liu, P., Kaplan, J. O., Mickley, L. J., Li, Y., Chellman, N. J., Arienzo, M. M., et al. (2021). Improved estimates of preindustrial biomass burning reduce the magnitude of aerosol climate forcing in the Southern Hemisphere. *Science Advances*, *7*(22), eabc1379. <https://doi.org/10.1126/sciadv.abc1379>
- Malavelle, F., Haywood, J., Jones, A., Gettelman, A., Clarisse, L., Bauduin, S., et al. (2017). Strong constraints on aerosol-cloud interactions from volcanic eruptions. *Nature*, *546*(7659), 485–491. <https://doi.org/10.1038/nature22974>
- Martins, J. V., Hobbs, P. V., Weiss, R. E., & Artaxo, P. (1998). Sphericity and morphology of smoke particles from biomass burning in Brazil. *Journal of Geophysical Research*, *103*(D24), 32051–32057. <https://doi.org/10.1029/98JD01153>
- Ming, Y., Ramaswamy, V., Donner, L. J., & Phillips, V. T. J. (2006). A new parameterization of cloud droplet activation applicable to general circulation models. *Journal of the Atmospheric Sciences*, *63*(4), 1348–1356. <https://doi.org/10.1175/jas3686.1>
- Ming, Y., Ramaswamy, V., Donner, L. J., Phillips, V. T. J., Klein, S. A., Ginoux, P. A., & Horowitz, L. W. (2007). Modeling the interactions between aerosols and liquid water clouds with a self-consistent cloud scheme in a general circulation model. *Journal of the Atmospheric Sciences*, *64*(4), 1189–1209. <https://doi.org/10.1175/jas3874.1>
- Mülmenstädt, J., & Feingold, G. (2018). The radiative forcing of aerosol-cloud interactions in liquid clouds: Wrestling and embracing uncertainty. *Current Climate Change Reports*, *4*(1), 23–40. <https://doi.org/10.1007/s40641-018-0089-y>
- Myhre, G., Samset, B. H., Schulz, M., Balkanski, Y., Bauer, S., Bernsten, T. K., et al. (2013). Radiative forcing of the direct aerosol effect from AeroCom Phase II simulations. *Atmospheric Chemistry and Physics*, *13*(4), 1853–1877. <https://doi.org/10.5194/acp-13-1853-2013>
- Naik, V., Horowitz, L. W., Fiore, A. M., Ginoux, P., Mao, J., Aghedo, A. M., & Levy, H. (2013). Impact of preindustrial to present-day changes in short-lived pollutant emissions on atmospheric composition and climate forcing. *Journal of Geophysical Research: Atmospheres*, *118*, 8086–8110. <https://doi.org/10.1002/jgrd.50608>
- Naoe, H., & Okada, K. (2001). Mixing properties of submicrometer aerosol particles in the urban atmosphere—With regard to soot particles. *Atmospheric Environment*, *35*(33), 5765–5772. [https://doi.org/10.1016/s1352-2310\(01\)00367-3](https://doi.org/10.1016/s1352-2310(01)00367-3)
- Okada, K., Ikegami, M., Zaizen, Y., Tsutsumi, Y., Makino, Y., Jensen, J. B., & Gras, J. L. (2005). Soot particles in the free troposphere over Australia. *Atmospheric Environment*, *39*(28), 5079–5089. <https://doi.org/10.1016/j.atmosenv.2005.05.015>
- Paulot, F., Paynter, D., Ginoux, P., Naik, V., & Horowitz, L. W. (2018). Changes in the aerosol direct radiative forcing from 2001 to 2015: Observational constraints and regional mechanisms. *Atmospheric Chemistry and Physics*, *18*(17), 13265–13281. <https://doi.org/10.5194/acp-18-13265-2018>
- Paynter, D. J., & Ramaswamy, V. (2012). Variations in water vapor continuum radiative transfer with atmospheric conditions. *Journal of Geophysical Research*, *117*, D16310. <https://doi.org/10.1029/2012JD017504>
- Paynter, D. J., & Ramaswamy, V. (2014). Investigating the impact of the shortwave water vapor continuum upon climate simulations using GFDL global models. *Journal of Geophysical Research: Atmospheres*, *119*, 10720–10737. <https://doi.org/10.1002/2014JD021881>
- Pincus, R., Forster, P. M., & Stevens, B. (2016). The Radiative Forcing Model Intercomparison Project (RFMIP): Experimental protocol for CMIP6. *Geoscientific Model Development*, *9*(9), 3447–3460. <https://doi.org/10.5194/gmd-9-3447-2016>
- Pincus, R., Mlawer, E. J., Oreopoulos, L., Ackerman, A. S., Baek, S., Brath, M., et al. (2015). Radiative flux and forcing parameterization error in aerosol-free clear skies. *Geophysical Research Letters*, *42*, 5485–5492. <https://doi.org/10.1002/2015GL064291>
- Pósfai, M., Simonics, R., Li, J., Hobbs, P. V., & Buseck, P. R. (2003). Individual aerosol particles from biomass burning in southern Africa: 1. Compositions and size distributions of carbonaceous particles. *Journal of Geophysical Research*, *108*(D13), 8483. <https://doi.org/10.1029/2002JD002291>
- Ramaswamy, V., Collins, W., Haywood, J., Lean, J., Mahowald, N., Myhre, G., et al. (2019). Radiative forcing of climate: The historical evolution of the radiative forcing concept, the forcing agents and their quantification, and applications. *Meteorological Monographs*, *59*, 14.1–14.101. <https://doi.org/10.1175/amsmonographs-d-19-0001.1>
- Rasch, P. J., Collins, W. D., & Eaton, B. E. (2001). Understanding the Indian Ocean Experiment (INDOEX) aerosol distributions with an aerosol assimilation. *Journal of Geophysical Research*, *106*(D7), 7337–7355. <https://doi.org/10.1029/2000JD900508>
- Regayre, L. A., Johnson, J. S., Yoshioka, M., Pringle, K. J., Sexton, D. M. H., Booth, B. B. B., et al. (2018). Aerosol and physical atmosphere model parameters are both important sources of uncertainty in aerosol ERF. *Atmospheric Chemistry and Physics*, *18*(13), 9975–10006. <https://doi.org/10.5194/acp-18-9975-2018>
- Regayre, L. A., Pringle, K. J., Booth, B. B. B., Lee, L. A., Mann, G. W., Browse, J., et al. (2014). Uncertainty in the magnitude of aerosol-cloud radiative forcing over recent decades. *Geophysical Research Letters*, *41*, 9040–9049. <https://doi.org/10.1002/2014GL062029>
- Rodhe, H., Persson, C., & Akesson, O. (1972). An investigation into regional transport of soot and sulfate aerosols. *Atmospheric Environment*, *6*(9), 675–693. [https://doi.org/10.1016/0004-6981\(72\)90025-x](https://doi.org/10.1016/0004-6981(72)90025-x)
- Russell, P. B., & Heintzenberg, J. (2000). An overview of the ACE-2 clear sky column closure experiment (CLEARCOLUMN). *Tellus*, *52B*(2), 463–483. <https://doi.org/10.1034/j.1600-0889.2000.00013.x>
- Schwarzkopf, M. D., & Ramaswamy, V. (1999). Radiative effects of CH₄, N₂O, halocarbons and the foreign-broadened H₂O continuum: A GCM experiment. *Journal of Geophysical Research*, *104*(D8), 9467–9488. <https://doi.org/10.1029/1999JD900003>
- Sherwood, S. C., Bony, S., Boucher, O., Bretherton, C., Forster, P. M., Gregory, J. M., & Stevens, B. (2015). Adjustments in the forcing-feedback framework for understanding climate change. *Bulletin of the American Meteorological Society*, *96*(2), 217–228. <https://doi.org/10.1175/bams-d-13-00167.1>
- Smith, C. J., Kramer, R. J., Myhre, G., Alterskjær, K., Collins, W., Sima, A., et al. (2020). Effective radiative forcing and adjustments in CMIP6 models. *Atmospheric Chemistry and Physics*, *20*(16), 9591–9618. <https://doi.org/10.5194/acp-20-9591-2020>
- Stevens, B. (2015). Rethinking the lower bound on aerosol radiative forcing. *Journal of Climate*, *28*(12), 4794–4819. <https://doi.org/10.1175/jcli-d-14-00656.1>
- Szopa, S., Naik, V., Adhikary, B., Artaxo, P., Bernsten, T., Collins, W. D., et al. (2021). Short-lived climate forcers. In V. Masson-Delmotte, P. Zhai, A. Pirani, S. L. Connors, C. Péan, S. Berger, et al. (Eds.), *Climate change 2021: The physical science basis. Contribution of working group I to the sixth assessment report of the intergovernmental panel on climate change* (pp. 817–922). Cambridge University Press. <https://doi.org/10.1017/9781009157896.008>

- Whitby, K. (1978). The physical characteristics of sulfate aerosols. *Atmospheric Environment*, *12*(1–3), 135–159. [https://doi.org/10.1016/0004-6981\(78\)90196-8](https://doi.org/10.1016/0004-6981(78)90196-8)
- Wilcox, L. J., Highwood, E. J., Booth, B. B. B., & Carslaw, K. S. (2015). Quantifying sources of inter-model diversity in the cloud albedo effect. *Geophysical Research Letters*, *42*, 1568–1575. <https://doi.org/10.1002/2015GL063301>
- Zelinka, M. D., Andrews, T., Forster, P. M., & Taylor, K. E. (2014). Quantifying components of aerosol-cloud-radiation interactions in climate models. *Journal of Geophysical Research: Atmospheres*, *119*, 7599–7615. <https://doi.org/10.1002/2014JD021710>
- Zelinka, M. D., Myers, T. A., McCoy, D. T., Po-Chedley, S., Caldwell, P. M., Ceppi, P., et al. (2020). Causes of higher climate sensitivity in CMIP6 models. *Geophysical Research Letters*, *47*, e2019GL085782. <https://doi.org/10.1029/2019GL085782>
- Zhao, M., Golaz, J.-C., Held, I. M., Guo, H., Balaji, V., Benson, R., et al. (2018a). The GFDL global atmosphere and land model AM4.0/LM4.0: 1. Simulation characteristics with prescribed SSTs. *Journal of Advances in Modeling Earth Systems*, *10*, 691–734. <https://doi.org/10.1002/2017MS001208>
- Zhao, M., Golaz, J.-C., Held, I. M., Guo, H., Balaji, V., Benson, R., et al. (2018b). The GFDL global atmosphere and land model AM4.0/LM4.0: 2. Model description, sensitivity studies, and tuning strategies. *Journal of Advances in Modeling Earth Systems*, *10*, 735–769. <https://doi.org/10.1002/2017MS001209>